Investigation of stress induced by CO_2 laser processing of fused silica optics for laser damage growth mitigation

Laurent Gallais,[1,*] Philippe Cormont,[2] Jean-Luc Rullier[2]

[1]*Institut Fresnel, CNRS, Aix-Marseille Université, Ecole Centrale Marseille, Campus de Saint-Jérôme, 13013 Marseille, France*
[2]*CEA CESTA, F-33114 Le Barp, France*
[*]*laurent.gallais@fresnel.fr*

Abstract: 'Laser damage mitigation' is a process developed to prevent the growth of nanosecond laser-initiated damage sites under successive irradiation. It consists of re-fusing the damage area with a CO_2 laser. In this paper we investigate the stress field created around mitigated sites which could have an influence on the efficiency of the process. A numerical model of CO_2 laser interaction with fused silica is developed. It takes into account laser energy absorption, heat transfer, thermally induced stress and birefringence. Residual stress near mitigated sites in fused silica samples is characterized with specific photoelastic methods and theoretical data are compared to experiments. The stress distribution and quantitative values of stress levels are obtained for sites treated with the CO_2 laser in various conditions of energy deposition (beam size, pulse duration, incident power). The results provided evidence that the presence of birefringence/residual stress around the mitigated sites has an effect on their laser damage resistance.

OCIS codes: (140.3330) Laser damage ; (160.6030) Silica .

References and links

1. J. Neauport, L. Lamaignere, H. Bercegol, F. Pilon and J.-C. Birolleau, "Polishing-induced contamination of fused silica optics and laser induced damage density at 351 nm," Opt. Express **13**, 10163-10171 (2005).
2. S. G. Demos, M. Staggs, and M. R. Kozlowski, "Investigation of processes leading to damage growth in optical materials for large-aperture lasers," Appl. Opt. **41**, 3628-3633 (2002).
3. R. M. Brusasco, B. M. Penetrante, J. A. Butler and L. W. Hrubes, "Localized CO_2 laser treatment for mitigation of 351 nm damage growth on fused silica," Proc. SPIE **4679**, 40-47 (2002).
4. R. Prasad, J. Bruere, J. Peterson, J. Halpin, M. Borden and R. Hackel, "Enhanced performance of large of optics using UV and IR lasers," Proc. SPIE **5273**, 288-295 (2003).
5. M. D. Feit and A. M. Rubenchik, "Mechanisms of CO_2 laser mitigation of laser damage growth in fused silica," Proc. SPIE **4932**, 91-102 (2003).
6. M. D. Feit, A. M. Rubenchik, C. D. Boley and M. Rotter, "Development of a process model for CO_2 laser mitigation of damage growth in fused silica," Proc. SPIE **5273**, 145-154 (2004).
7. E. Mendez, K.M. Nowak, H. J. Baker, F. J. Villareal and D. R. Hall, "Localized CO_2 laser damage repair of fused silica optics," Opt. Express **45**, 5358-5367 (2006).
8. G. Guss, I. Bass, V. Draggoo, R. Hackel, S. Payne, M. Lancaster and P. Mak, "Mitigation of growth of laser initiated surface damage in fused silica using a 4.6 µm wavelength laser," Proc. SPIE **6403**, 64030M (2007).
9. S. Palmier, L. Gallais, M. Commandré, P. Cormont, R. Courchinoux, L. Lamaignère, J-L Rullier and P. Legros "Optimization of a laser mitigation process in damaged fused silica," Appl. Surface Science **255**, 5532-5536 (2008).
10. I. L. Bass, G. M. Guss and R. P. Hackel, "Mitigation of laser damage growth in fused silica with a galvanometer scanned CO_2 laser," Proc. SPIE **5991**, C9910-C9910 (2005).
11. A. During, P. Bouchut, J. G. Coutar, C. Leymarie and H. Bercegol, "Mitigation of laser damage on fused silica surfaces with a variable profile CO_2 laser beam," Proc. SPIE **6403**, 40323-40323 (2007).
12. S. G. Demos, M. Staggs, K. Minoshima, and J. Fujimoto, "Characterization of laser induced damage sites in optical components," Opt. Express **10**, 1444-1450 (2002).

#116211 - $15.00 USD Received 25 Aug 2009; revised 15 Oct 2009; accepted 16 Oct 2009; published 8 Dec 2009

13. G. Guss, I. Bass, R. Hackel, C. Mailhiot and S. Demos, "In situ monitoring of surface post processing in large-aperture fused silica optics with optical coherent tomography," Appl. Opt. **47**, 4569-4576 (2008).
14. B. Bertussi, P. Cormont, S. Palmier, P. Legros and J.-L. Rullier, "Initiation of laser-induced damage sites in fused silica optical components," Opt. Express **17**, 11469-11479 (2009).
15. M. A. Stevens-Kalceff and J. Wong, "Distribution of defects induced in fused silica by ultraviolet laser pulses before and after treatment with a CO_2 laser," J. Appl. Phys. **97**, 113519 (2005).
16. S. Mainguy and B. Le Garrec, "Propagation of LIL/LMJ beams under the interaction with contamination particles and component surface defects," J. de Phys. IV **133**, 653-655 (2006).
17. M. J.Matthews, I. L. Bass, G. M. Guss, C. C Widmayer and F. L. Ravizza, "Downstream intensification effects associated with CO_2 laser mitigation of fused silica," Proc. SPIE **6720**, A7200-A7200 (2008).
18. L. Lamaignère,S. Bouillet, R. Courchinoux, T. Donval, M. Josse, J.-C. Poncetta, and H. Bercegol, "An accurate, repeatable, and well characterized measurement of laser damage density of optical materials," Rev. Scientific Instruments **78**, 103105 (2007).
19. M. Von Allmen, *Laser-beam interactions with material*, (Spinger-Verlag, 1987).
20. A. D. McLachlan and F. P. Meyer, "Temperature dependence of the extinction coefficient of fused silica for CO_2 laser wavelengths," Appl. Opt. **26**, 1728-1731 (1987).
21. http://optics.heraeus-quarzglas.com
22. http://www.comsol.com/
23. J. Zarzyski, "Les verres et l'état vitreux", Masson (1982).
24. S. Huard, *Polarization of light*, (John Wiley and Sons, 1997).
25. Y. S. Touloukian, "Thermo-physical propoerties of matter vol.3 – Thermal conductivity of liquids and gases," IFI/Plenum, 1970.
26. F. Dahmani, J.C. Lambropoulos, A. W. Schmid, S. Papernov and S. J. Burns, "Crack Arrest and Stress Dependence of Laser-Induced Surface Damage in Fused-Silica and Borosilicate Glass," Appl. Opt. **38**, 6892-6903 (1999).
27. L. Xu, D. Lowney, P. J. McNally, A. Borowiec, A. Lankinen, T. O. Tuomi and A. N. Danilewsky, "Femtosecond versus nanosecond laser micro-machining of InP: a nondestructive three-dimensional analysis of strain," Semicond. Sci. Technol. **22**, 970–979 (2007).

1. Introduction

Laser damage of optical components is a main issue for high power laser systems. Particularly for ICF class lasers, the laser damage resistance of fused silica surfaces at 351 nm in the nanosecond regime is a major concern. Indeed such facilities involve many large and high-cost elements, such as windows, lenses, crystals, diffractive optical elements...etc. Although the polishing techniques of silica have been considerably improved, defects that can initiate damage are still present in the material [1]. Laser irradiations of these weak points lead to stress, cracks and absorption. The created damage grows under subsequent irradiations and makes the component unsuitable [2]. To avoid damage site growth, one of the most promising methods uses a CO_2 laser operating at a 10.6 µm wavelength to locally melt and evaporate the silica surface by producing typically smooth, Gaussian shaped pits [3]. The successful demonstration of this method [4] motivates theoretical and experimental work to improve the process. For instance, the influence of irradiation parameters with models taking into account heating, evaporation and stress generation has been studied [5,6]. Some parametric studies have been conducted in order to determine optimum irradiation conditions [7-9] and different protocols have been developed to increase the efficiency of the technique [10,11]. Dedicated tools have also been developed to characterize the damages sites and the mitigated area [12-14]. The material structural changes induced by CO_2 laser processing of damage have also been investigated [15]. Other studies on the downstream intensification effects associated with the perturbation to the optical surface profile following the mitigation process were also conducted [16,17].

In this context, it has been observed that after 355 nm irradiation, of a zone that has received CO_2 laser treatment, new damages always occur in the surrounding area of the crater, even when the surface is free from any visible defects or silica re-deposition. The understanding of the silica weakening and the apparition of damage around the mitigated site is then of major interest for the optimization of the mitigation process. This motivation was completed by the observation that the same effect is obtained when a crater is created on a blank sample with no initial damage. The objective of our work is then, to investigate the stress generated around the mitigated sites, of an un-damaged silica sample, by the heating

#116211 - $15.00 USD Received 25 Aug 2009; revised 15 Oct 2009; accepted 16 Oct 2009; published 8 Dec 2009

and cooling process, and study its influence on the laser damage resistance of the treated sites. Another motivation of this work is that the link between laser damage and local stress is still unclear.

To address this issue, first the experimental details of stress measurements and laser damage testing are given, with a focus on the different photoelastic tools that have been implemented for this study. Secondly, we describe a simple model to obtain the stress distribution in the CO_2 heated material that we have developed for the interpretation of photoelastic measurements. Finally, calculated values of stresses and strains around the mitigated sites are compared with experiments, and the stress influence on the laser damage resistance is discussed.

2. Experiments

The samples under investigation in this study are specimen of UV fused silica (Corning 7980), polished by SESO, 50 mm in diameter, and 5 mm thick. On these blank samples, craters were created by CO_2 laser irradiation with various parameters (power, irradiation time, beam diameter). Laser damage tests were performed to analyze the damage initiation process on these sites and the residual stress field around the craters was characterized with photoelastic tools. For each set of parameters, 30 craters were created and analyzed. The results given in this paper are then based on a statistical analysis on these samples.

2.1 CO_2 Laser mitigation procedure

The CO_2 laser used for silica irradiation is a Synrad Firestar V20, operating at 10.6 µm wavelength with a 20 W maximum power. The beam is focused with a ZnSe lens with a 10 in. focal length. The latter is mounted on a z translation stage to adjust the beam diameter on the sample from 200 µm to 800 µm measured at $1/e^2$. More details about the experimental arrangement can be found in reference [9].

The irradiation conditions were adjusted to create 20 µm to 50 µm deep craters, which corresponds to the depth of typical damages that we need to treat for the laser mitigation process of LMJ optics [14]. The different set of parameters that were used in this study, with the corresponding crater dimensions are listed in table 1.

Table 1: Details of the different irradiation conditions and dimensional characteristics of the CO_2-craters studied. The crater dimensions are measured with an optical profiler.

	Irradiation parameters			Crater dimensions	
Case	Diameter ($1/e^2$)	Pulse duration	Power	Diameter	Depth
1	300 µm	0.25 s	2.5 W	130 µm	24 µm
2	300 µm	1 s	2.5 W	145 µm	35 µm
3	460 µm	0.25 s	3.4 W	150 µm	25 µm
4	460 µm	1 s	3.4 W	180 µm	43 µm
5	550 µm	0.25 s	4.5 W	180 µm	27 µm
6	550 µm	1 s	4.5 W	260 µm	54 µm

2.2 Laser damage tests procedure and results

Laser damage resistance tests are performed with a Nd:YAG table-top laser, which delivers a pulse length of 2.5 ns at 355 nm with a diameter of 0.9 mm at $1/e^2$ at the sample surface [18]. The beam is centered on the crater to be tested and the fluence is increased until damage

#116211 - $15.00 USD Received 25 Aug 2009; revised 15 Oct 2009; accepted 16 Oct 2009; published 8 Dec 2009

occurs. The damage detection is made *in situ* by monitoring a scattering signal, completed with a mobile macroscope.

On the different craters that were created with the parameters given above, damages were systematically initiated in an area surrounding the crater. An illustration of this behavior is given in Fig. 1a, and the part b of the figure shows that even after damage growth the localization follows a circle.

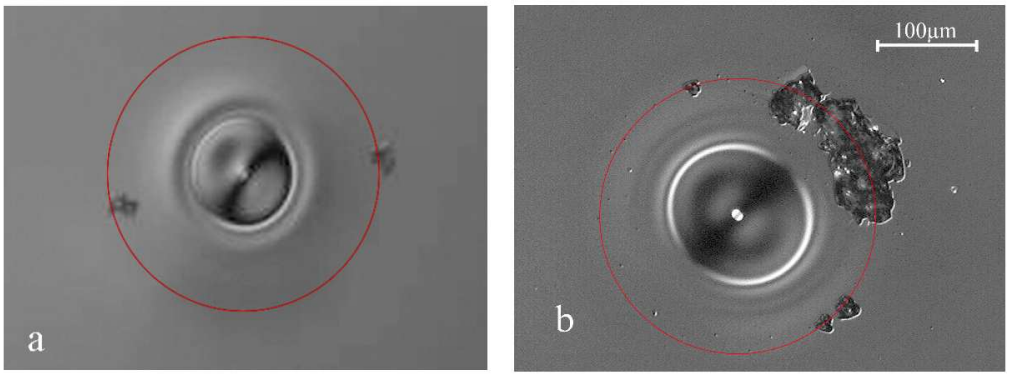

Fig. 1. Observation by Nomarski microscopy of mitigated sites after the laser damage test procedure. a- after one shot at 11J/cm², b- after 10 shots at 11J/cm². The red circle is plotted to evidence the circular symmetry of the damage appearance.

As indicated by the red circle, the location of the 'weak' area regarding the laser damage resistance is circular and centered on the crater. For the different cases that we have tested, similar behavior has been obtained. Moreover, we have observed that this "damage initiation diameter" depends on the parameters used to create the crater. The relationship between this diameter (ϕ_{damage}) and the crater diameter (ϕ_{crater}) is given in Fig. 2.

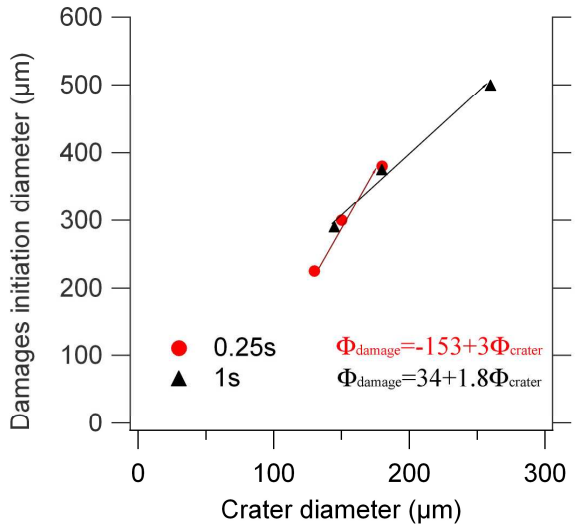

Fig. 2. Relation between the "damage initiation diameter" and the crater diameter.

These measurements reveal for each pulse length a clear proportionality between the "damage initiation diameter" and the crater dimension. A factor 3 and 1.8 are respectively found for 0.25s and 1s length of irradiation.

#116211 - $15.00 USD Received 25 Aug 2009; revised 15 Oct 2009; accepted 16 Oct 2009; published 8 Dec 2009

If the laser damage tests permit us to delineate this 'weak' area, no indication on the origin of the weakness can be obtained with this test. Different investigations conducted by Nomarski and dark field microscopy have not shown any correlation between visible defects or contaminants due to silica evaporation and location of the damages. Indeed, whereas the surrounding area of the crater is uniformly polluted on an area extending far away form the crater, damage occurs at a precise location.

2.3 Photoelastic measurement setup and results

The laser processing of silica involves heating at high temperature and rapid cooling which can produce some stress in the material. We have therefore implemented some tools to evaluate the stress and study its potential correlations with laser damage. Since we are investigating a transparent material, a photoelastic method was chosen for evaluating and measuring the stresses around the mitigated sites. The method is based on the property of birefringence which is exhibited by certain transparent materials under stress. It consists in measuring the phase retardation, and hence the refractive indices, between two waves polarized along two directions of stress. The advantages of such methods is that they are non-invasive and do not necessitate any preparation of the samples.

Two complementary experimental set-ups were developed to localize the stress area and to measure quantitatively the birefringence. The first one is a polariscope, described in Fig. 3. The silica sample, illuminated with a collimated white light source, is placed between two cross polarizers and observed with a long working distance microscope associated to a cooled camera. The microscope is a BXFM from Olympus.

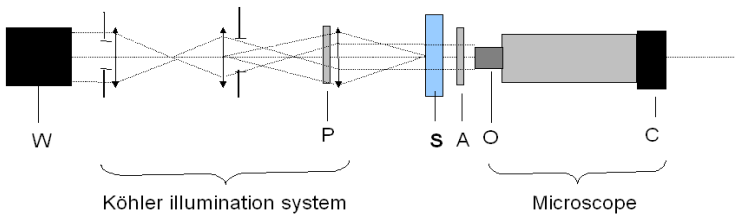

Fig. 3. Polariscope developed for the observation of mitigated sites. W: White light collimated source, P/A: high contrast polarizer and analyzer (10000:1); S: silica sample; C: Camera (12.5 million-pixel, 12-bits, cooled color camera), O: long working distance objective (X10).

In this configuration, the stress-induced anisotropy in the sample will result in a light pattern associated to the stress distribution. An example of the pattern observed when looking at mitigated sites with this setup is given in Fig. 4.

#116211 - $15.00 USD Received 25 Aug 2009; revised 15 Oct 2009; accepted 16 Oct 2009; published 8 Dec 2009

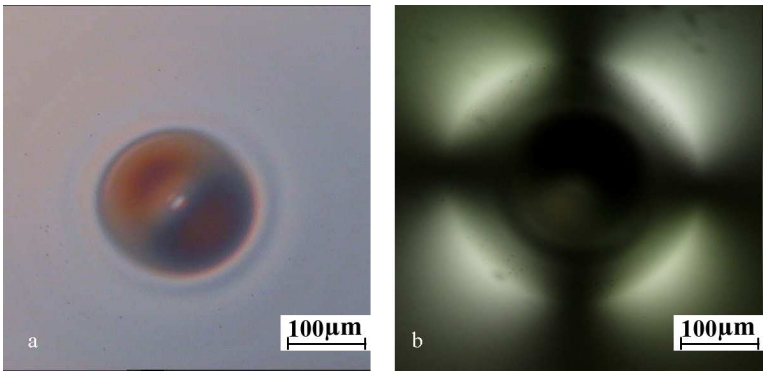

Fig. 4. Observation of a mitigated site, with parameters of the case 4, by Nomarski microscopy (a) and with the polariscope (b).

A maximum of retardance is evidenced around the crater, and from this position the retardance decreases rapidly in the inner part, and decreases slowly on the outer part. The measured retardance in the different cases under study is less than one wavelength.

Because of the structure of the crater the stress distribution has an azimuthal symmetry. The directions of principal stresses are parallel or orthogonal to the radius as represented in Fig. 5a. The local birefringence depends on the difference between these two principal stresses. When the light is polarized along a stress direction it remains linearly polarized and no light can pass through the cross polarizer, which happens for four different directions as shown in Fig. 5b. On the contrary a maximum retardance occurs when the light is polarized at 45° with respect to the two principal stress directions, which describes the pattern observed in Fig. 4b.

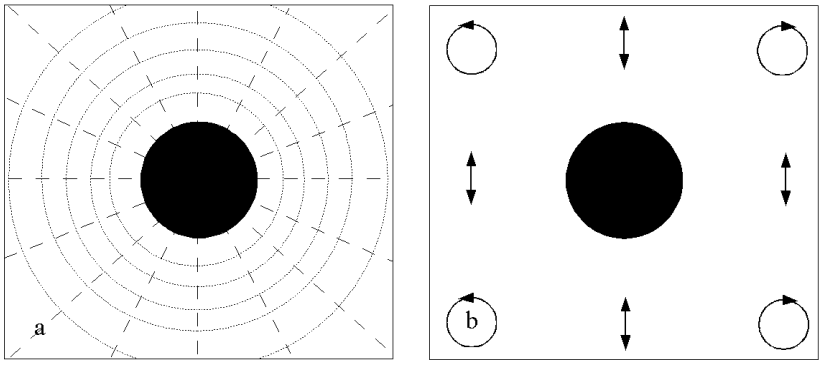

Fig. 5. a.The principal directions of the stress around the mitigated site, which are either parallel or orthogonal to the radius. b. Schematic representation of the resulting polarization state at the output of a mitigated site for incident light linearly polarized in the vertical direction.

The measurements made on the cases under study reveal that the craters have comparable stress pattern characteristics but the maximum retardance have location and magnitude depends on the irradiation parameters. The location of the "maximum retardance diameter" ($\phi_{max\ ret}$) has been evaluated by analyzing microscope images and related to the crater diameter (ϕ_{crater}) in Fig. 6.

#116211 - $15.00 USD Received 25 Aug 2009; revised 15 Oct 2009; accepted 16 Oct 2009; published 8 Dec 2009

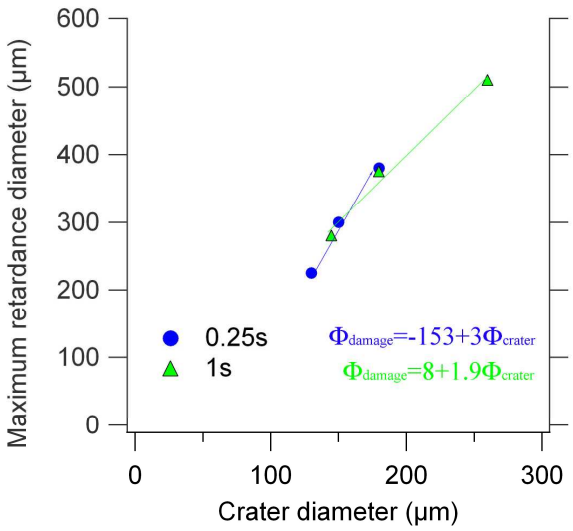

Fig. 6. Relation between the "maximum retardance diameter" and the crater diameter.

As previously observed for the damage position, for each pulse length a linear relationship links the "maximum retardance diameter" and the crater diameter. By comparing these results with those of the Fig. 2, it appears clearly that damage is initiated close to the location where the retardance is maximum. This relation is obvious when one looks at the damaged craters under the polariscope. In Fig. 7, two extreme parameter conditions, more representative than the 6 cases under study, are shown. They indicate unequivocally that the damage occurs at a radius where the retardance is maximum. This happens regardless of whether the radius is large or small as shown in the Fig. 7.

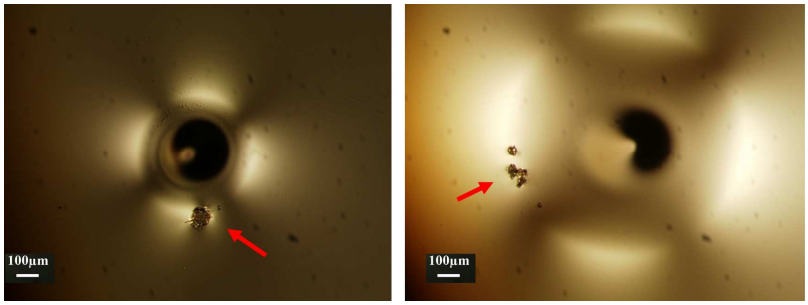

Fig. 7. Observation of two craters with the polariscope. The damages are indicated with the red arrows. Notice that the polarizers were not perfectly orthogonal in order to image simultaneously the sample surface and the stress field.

Since polariscope is not suitable for obtaining a calibrated measure of retardance, a second setup, described in Fig. 8, has been implemented. A polarized He-Ne laser beam is focused on the sample surface with approximately 5 µm diameter. A second lens is used to collimate the beam before passing through a Soleil-Babinet compensator. The retardation of the compensator is adjusted to reduce to zero the amount of light passing through the analyzer oriented perpendicular to the input polarization. In this configuration the retardation induced by the sample can be obtained. The sample being mounted on a XY translation stage, the birefringence can be measured at different locations.

#116211 - $15.00 USD Received 25 Aug 2009; revised 15 Oct 2009; accepted 16 Oct 2009; published 8 Dec 2009

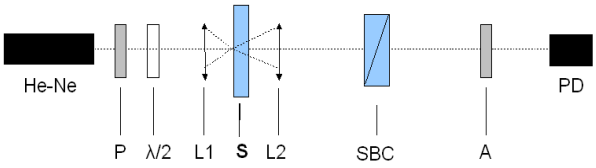

Fig. 8. Experimental setup for measuring birefringence with a Soleil-Babinet compensator (SBC). He-Ne: 0.5mW Helium-Neon Laser; P/A: high contrast polarizer and analyzer (10000:1); λ/2: half wave plate; L1: microscope objective (X20); S: silica sample; L2: microscope objective (X10).

The maximum retardance has been measured with the compensator setup, for the 6 cases studied. The results are given in Fig. 9 as a function of the crater depth.

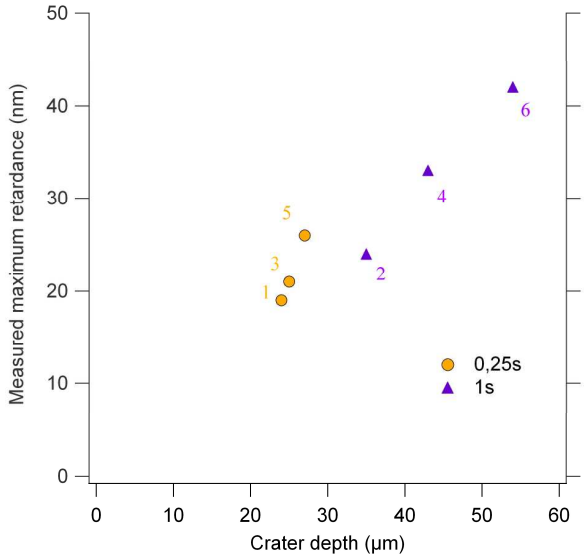

Fig. 9. Relation between the maximum retardance measured and the crater depth for the 6 cases under study.

These measurements show that the maximum retardance measured depends strongly on the irradiation parameters. As for the location of the maximum retardance, for each pulse length a quasi-linear relation links the quantitative value of the maximum retardance with the crater depth. The retardance value is associated to the stress level that we want to evaluate. However, there is no direct proportionality between the retardance and the stress level since the retardance is integrated over the thickness of the sample. Hence a low level of stress extending far from the surface and a high level of stress near the surface can lead to the same results. Thus a model is needed to obtain an interpretation of the measurements.

3. Theoretical analysis

In order to evaluate the temperature reached and the stresses generated during CO2 laser irradiation of fused silica, a numerical model has been developed. The objective of our approach is to be able to quantify the stresses, strains and induced birefringence generated around the crater by the mitigation process. Given the symmetry of the study, the geometry used to solve the heat equation is 2D axi-symmetric, as shown in Fig. 10.

#116211 - $15.00 USD Received 25 Aug 2009; revised 15 Oct 2009; accepted 16 Oct 2009; published 8 Dec 2009

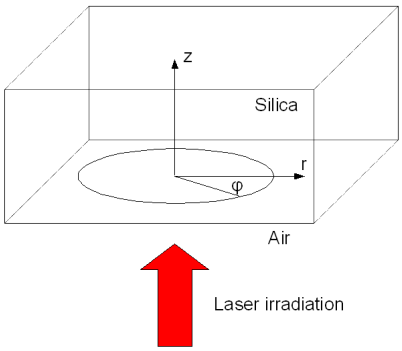

Fig. 10. Geometry used in the model

3.1 Temperature distribution

The energy of the CO_2 laser beam is absorbed by the silica. It generates a heat source Q during the irradiation time in the material. In our case of a Gaussian laser beam, the heat source can be expressed as [19]:

$$Q = \alpha \frac{(1-R)P}{\pi a^2} \exp\left(-\frac{r^2}{a^2}\right) \exp(-\alpha z) \qquad (1)$$

with a the radius waist at 1/e, P the incident laser power (considering a constant laser power during the irradiation time), R the Fresnel reflection coefficient and α the absorption coefficient. The absorption coefficient of silica at 10,6 µm is temperature dependent. To take into account this variation, we have used the experimental data reported by McLachlan and Meyer [20]. As concerns the Fresnel coefficient (which depends of the refractive index) we have not found any significant variation with the temperature in the literature.

To calculate the temperature distribution around a mitigated site, we have only considered heat transfer by conduction: radiation losses which occur at high temperature are taken into account with the non-linearity of the thermal conductivity with temperature. We do not consider in our calculation the evaporation of material during the irradiation, indeed this case is much more complex to model and we are only interested in the thermal gradient far from the center. Therefore the results obtained at the position where experimentally a crater is observed are not valid.

In the silica, the heat equation for conductive heat transfer is:

$$\rho C \frac{\partial T}{\partial t} + \nabla.(-k\nabla T) = Q \qquad (2)$$

where T is the temperature, ρ the density, C the heat capacity, and k the thermal conductivity. The thermal parameters of silica are temperature dependent. Particularly the thermal conductivity, which is the key parameter governing the temperature rise, increases with temperature. We have used in our simulations the data on fused silica given by glass manufacturers [21].

Finally, the equation is numerically solved using the commercial software COMSOL Multiphysics , version 3.2 [22]. The mesh element is triangular. Its surface is around 50µm² in the strongly heated area. This surface is increased when moving from this position up to 10^4µm² on the sample edges. Boundary condition is an inward heat flux on the surface exposed to laser, and thermal insulation on the other surfaces of the sample. A solution calculated for the case 3 of our study is given in Fig. 11.

#116211 - $15.00 USD Received 25 Aug 2009; revised 15 Oct 2009; accepted 16 Oct 2009; published 8 Dec 2009

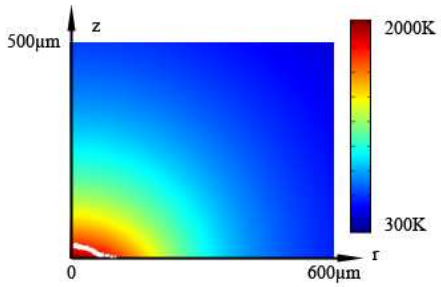

Fig. 11. Calculated temperature distribution in fused silica at the end of the CO_2 laser irradiation for parameters of the case 3. The crater is delimited by the white line.

From this calculation, it can be seen that the heated area extends far beyond from the crater dimensions delimited by the white line. The spatial distribution of temperature follows the crater shape, and decreases slowly with distance. It is important to notice that in the crater vicinity, the calculated temperature is not valid because the material removed as the crater is shaped is not included in our simple model.

3.2 Stress and strains

After laser heating, when the material cools down, the viscosity rapidly increases [23] and stresses cannot be relieved by materials displacements. It appears that whatever the irradiation parameters (for the six cases of our study) the area where the maximum retardance is experimentally observed corresponds to a calculated temperature reached at the end of the pulse between 1300 to 1400°C. These values have to be compared to the strain temperature (1100°C) and the softening temperature (1600°C) of fused silica [23]. The strain point is the temperature at which internal stress in a piece of glass is substantially relieved and the softening point corresponds to the transition from 'soft' to solid material. For low temperatures compared to these values the stresses can be considered as imprinted into the material after heating because of the very high viscosity. Then far away from the crater the residual stress present in the material corresponds to the stress at the end of the pulse. However near the center the stress can be relieved due to material displacement in the created hole. This could explain the retardance pattern experimentally observed.

In our approach the stresses are calculated at the end of the laser pulse. As said above, for temperatures below a limit between 1100 and 1600°C, the stresses can be treated as imprinted into the material. Thus we can only consider stress values obtained below this range of temperature. This is certainly a limitation, but it seems sufficient to deal with our problem since we are only interested in the stress field at a distance from the crater where the temperature rise is moderate.

The laser heating of the glass generates material displacements due to thermal expansion. The thermal expansion coefficient value of silica is $5\text{x}10^{-7}$ K^{-1} and does not vary significantly with temperature [21]. In our case the material displacement have components in the r and z directions that will be called u and w respectively**.** The strain-displacement relationships in the case of small displacements are given by:

$$\varepsilon_r = \frac{\partial u}{\partial r}; \varepsilon_\phi = \frac{u}{r}; \varepsilon_z = \frac{\partial w}{\partial z}; \gamma_{rz} = \frac{\partial u}{\partial z} + \frac{\partial w}{\partial r} \qquad (3)$$

with ε_r, ε_Φ, ε_z the strains in the r, Φ, z directions and γ_{rz} the shear strain in the r z plane. The stresses consisting of three normal stresses (σ_r, σ_φ, σ_z) and one shear stress (τ_{rz}), are related to the strains in the case of elastic deformation:

$$\sigma_{ij} = D_{ijkl}\varepsilon_{kl} \qquad (4)$$

#116211 - $15.00 USD Received 25 Aug 2009; revised 15 Oct 2009; accepted 16 Oct 2009; published 8 Dec 2009

with D_{ijkl} the elasticity tensor which depends on Young's modulus (E=7.2x10^{10} N.m^{-2}) and Poisson's ratio (υ=0.17) [23].

A solution calculated for the case 3 is given in Fig. 12.

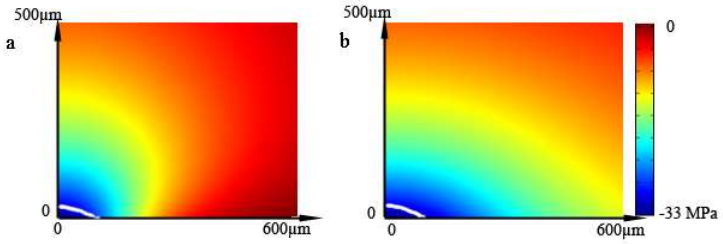

Fig. 12. Calculated hoop (a) and radial (b) stresses in fused silica at the end of the CO2 laser irradiation for the parameters of the case 3. The crater is delimited by the white line.

The calculations indicate that a compressive stress of few tens of Mpa can be reached under the irradiation conditions and that the stress affected area extends far away from the crater. However, near the crater, the stress can be relaxed after the irradiation because of the presence of the hole in the material (material displacement can occur) and the calculation is not valid.

3.3 Birefringence

To be able to compare our calculations with experimental results, we have to link in our model the stress to the retardation of linearly polarized plane waves traveling along the *z* direction, as it is the case in the experiments. If we consider a wave polarized in the *r* direction, called E_r, and the corresponding perpendicular polarization E_Φ, we can work for simplicity in the local Cartesian coordinates *x,y,z* as defined on the Fig. 13.

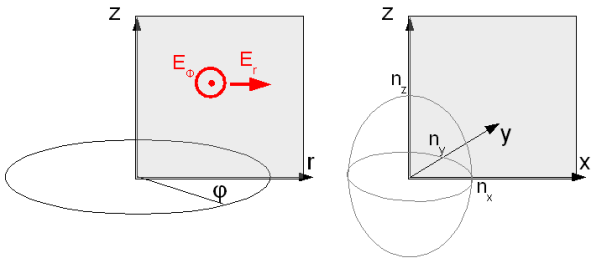

Fig. 13. Description of the index ellipsoïd as used in our calculation.

The coefficient refractive index of a material subject to elastic stress can be written in the local Cartesian coordinates defined above as [24]:

$$\frac{1}{n'^2_{ij}} = \left[\frac{1}{n'^2_{ij}}\right]_{[\sigma]=0} + \Delta\frac{1}{n^2_{ij}} \qquad (5)$$

with *i* and *j* = *x, y or z*.

The refractive index variations and the strains [ε] are related by the photoelastic tensor [*p*]:

$$\Delta\frac{1}{n^2_{ij}} = p_{ijmn}\varepsilon_{mn} \qquad (6)$$

In a first order approximation and considering the photoelastic tensor of an isotropic media [24], the refractive indices n_x and n_y can be expressed as:

$$n_x = n_0 - \frac{1}{2}n_0^3\left[p_{11}\varepsilon_x + p_{12}(\varepsilon_y + \varepsilon_z)\right] \qquad (7)$$

$$n_y = n_0 - \frac{1}{2}n_0^3\left[p_{11}\varepsilon_y + p_{12}(\varepsilon_x + \varepsilon_z)\right]$$

#116211 - $15.00 USD Received 25 Aug 2009; revised 15 Oct 2009; accepted 16 Oct 2009; published 8 Dec 2009

The birefringence B is defined as the difference of n_x and n_y refractive indices:

$$B = n_x - n_y = \frac{1}{2} n_0^3 \left[p_{11}(\varepsilon_x - \varepsilon_y) + p_{12}(\varepsilon_y - \varepsilon_x) \right] \tag{8}$$

with n_0=1.46 the stress-independent refractive index of fused silica at 0.633 µm, $p11$=0.121 and $p12$=0.270 at 0.633 µm for fused silica [24].

The retardance can be calculated:

$$\Gamma = \int_0^e B(z)dz \tag{9}$$

with e the sample thickness. The calculated retardance for the case 3 is finally given in Fig. 14.

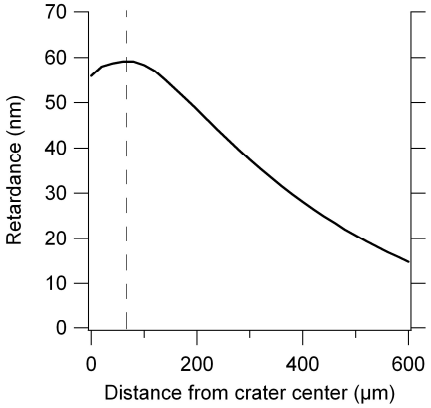

Fig. 14. Theoretical retardance for the case 3. The crater diameter is delimited by the dashed line.

As observed in experiments a maximum of retardance is observed near the crater, and from this position the retardance decreases slowly in the outter part of the crater. However the maximum is not at the right place compared to measured ones. The same behavior is observed for the other cases. This calculations will be compared to measurements in the next section.

4. Discussion

For the two CO_2 pulse lengths used in this study, a comparable behavior has been observed and we will restrict our discussion to the three cases using 250 ms duration. From the simple model developed in the preceding part of this paper, we can visualize for the fused silica surrounding the crater, the distribution of strains at the end of the CO_2 laser irradiation. In parallel, the experimental measurement presented earlier gave a precise position for the maximum retardance. Confrontations between experiment and simulation are then given in Fig. 15, where the measured maximum retardance (which is proportional to the integral of the difference of refractive indices along the dashed white line) is positioned on the calculated strain repartition. Each image corresponds to one of the case 1, 3 and 5 under study for both radial (a) and hoop (b) strains.

#116211 - $15.00 USD Received 25 Aug 2009; revised 15 Oct 2009; accepted 16 Oct 2009; published 8 Dec 2009

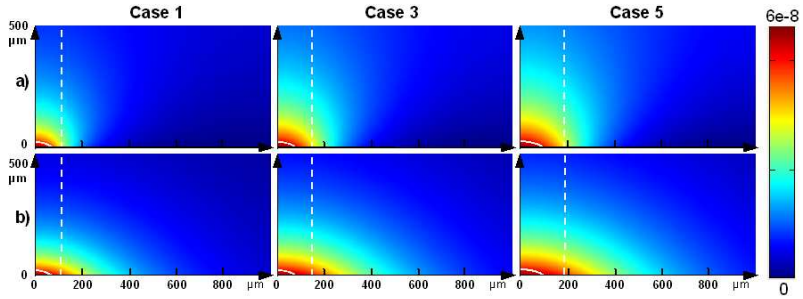

Fig. 15. Calculated strain repartition in fused silica at the end of the CO_2 laser irradiation for parameters of the three cases with a pulse length of 250 ms. Radial strains are represented on the upper part (a), and hoop at the lower (b). Craters sizes and positions of each maximum of retardance are indicated with a full and dashed white line respectively.

Similar behavior is obtained for the three cases, and the strain area expands following the increase in crater size. The hoop strain (b) decreases with distance from the crater. However, the contours of constant strain maintain a shape similar to the crater. The radial strain (a) also exhibits this behavior, but decreases much more rapidly along the silica-air interface. The position of the experimental maximum retardance corresponds to a distance from the center where the two calculated strains are noticeably different along the depth axis, but still with a high level . For the three cases 1, 3 and 5, their theoretical values are respectively 48, 53 and 55 nm, which is of the same order as experimental results given in Fig. 9 (19, 21 and 26 nm). As mentioned above, the crater area and its nearby proximity are not well simulated with our model, which explain that simulation values are greater by a factor comprised between 2.1 to 2.5. Taking into account the material removal, and a better kinetic of cooling for silica would reduce significantly this disagreement. In addition, some parameter values are not known perfectly: concerning the thermal conductivity, different experimental and theoretical data are available in the literature, sometimes with large discrepancies as can been observed in the data summarized by Touloukian [25].

On the one hand we know from the experiment that the maximum retardance position and the damage initiation are tightly correlated. On the other hand, Fig. 15 shows clearly that when the crater diameter increases, the maximum retardance gets farther from it and originates from a wider strain area. Thus for an equivalent value of retardance, we can look forward to a smaller effect on the damage creation for a larger crater size.

Laser damage resistance tests performed with our Nd:YAG laser at a fluence of 11 J/cm^2, show that only 10 % of crater sites were damaged in the case 5 where the maximum retardance was measured at 190 µm from the crater center, whereas more than 80 % are damaged in the case 1 for which the distance is 130 µm. For the intermediate case 3, about 20 % of sites are damaged at a distance of 150 µm.

Even if these results seem to confirm our hypothesis, they are not sufficient to conclude at a direct connection between damage initiation and silica stress. Indeed, for the three cases, although an unambiguous difference is obtain for the damage initiation, the stress values at the position of the maximum retardance and at the silica surface (where damages arise) are comparable: about 25 Mpa for the radial, and comprised between 15 and 20 Mpa for the hoop. Our study indicates a clear link between the stress and the laser damage resistance. Previous works by Dahmani et al. [26] have also shown a relationship between stress and laser-induced damage in silica (in their case an enhancement of threshold with external applied stress). However the physical mechanisms implied are unclear and still more work are needed to investigate the relationship between the stress level and the laser damage initiation.

5. Conclusion

As mentioned in the introduction of this paper, the objective of our work was the understanding of the silica weakening and re-initiation of damage around the mitigated sites.

#116211 - $15.00 USD Received 25 Aug 2009; revised 15 Oct 2009; accepted 16 Oct 2009; published 8 Dec 2009

We have realized an experiment focusing on six different CO_2 laser parameters. We have shown that for all the six cases, that have been irradiated with a Nd:YAG nanosecond laser, the damage initiation has occurred on a peripheral area free from any visible defects and submitted to a high level of stress. In order to estimate the stress value in this area and understand the potential weakness of the material, we have measured the retardance and a model has been established to link the retardance to the stress. From these results, it comes out that even if the theoretical and experimental values are of the same order of magnitude there is an overestimation of the retardance with our model. However, these results can be very useful since they give a good indication of the stress levels induced by the CO_2 laser processing of fused silica: few tens of Mpa of compressive stress occurring near the surface at a distance of twice the crater size (in our irradiation conditions).

We have evidenced a correlation between the place where damage takes place and the location of the maximal residual retardance around the mitigated site. Then again an extensive work that we will consider in a near future involving local analysis (micro-Raman spectrocopy for instance is well adapted [27]) associated with an accurate metrology of LIDT is needed to understand the potential mechanisms that can be involved. Also, we have developed a thermo-mechanical model of CO_2 laser interaction with fused silica with applications in the optimization of the mitigation of damage growth process. The perspectives on this point are now to take into account the material removal by evaporation and recalculate the stresses more accurately.

#116211 - $15.00 USD Received 25 Aug 2009; revised 15 Oct 2009; accepted 16 Oct 2009; published 8 Dec 2009